APL Energy

RESEARCH ARTICLE | SEPTEMBER 05 2023

Role of nanoscale compositional inhomogeneities in limiting the open circuit voltage in $Cu(In,Ga)S_2$ solar cells

Sean Peedle ; Damilola Adeleye ; Sudhanshu Shukla ; Susanne Siebentritt ; Rachel Oliver ; Gunnar Kusch

Check for updates

APL Energy 1, 026104 (2023)
https://doi.org/10.1063/5.0145450

View Online
Export Citation
CrossMark

05 September 2023 12:41:40

AIP Publishing

Role of nanoscale compositional inhomogeneities in limiting the open circuit voltage in $Cu(In,Ga)S_2$ solar cells

Cite as: APL Energy 1, 026104 (2023); doi: 10.1063/5.0145450
Submitted: 6 February 2023 • Accepted: 24 July 2023 •
Published Online: 5 September 2023

View Online Export Citation CrossMark

Sean Peedle,[1] Damilola Adeleye,[2] Sudhanshu Shukla,[2] Susanne Siebentritt,[2,a)] Rachel Oliver,[1] and Gunnar Kusch[1]

AFFILIATIONS

[1] Department of Materials Science and Metallurgy, Cambridge University, Cambridge CB3 0FS, United Kingdom
[2] Laboratory for Photovoltaics, Department of Physics and Materials Science Research Unit, University of Luxembourg, 44 Rue du Brill, 4422 Belvaux, Luxembourg

[a)] Author to whom correspondence should be addressed: susanne.siebentritt@uni.lu

ABSTRACT

As Si-based solar cell technologies approach their theoretical efficiency limits, alternative photovoltaic systems, such as tandem solar cells, are gathering increased attention due to their potential to reach higher efficiencies by better use of the solar spectrum. $Cu(In,Ga)S_2$ (CIGS) is a promising material for the top cell due to its large, tunable bandgap energy (E_g), stability, and already established high efficiencies. However, the deficit in open circuit voltage is still large; therefore, an improved understanding of the efficiency losses is required. Scanning electron microscopy cathodoluminescence was used to study the role of the polycrystalline nature for radiative recombination in CIGS samples of varying Cu-content. Considerable differences between neighboring grains were observed in the emission energy and the emission intensity, with significant drops in emission energy at the grain boundaries. Lateral homogeneity in the near band edge (NBE) energy was found to reduce for samples with Cu-poor compositions, with its standard deviation halving ($\sigma_{NBE} \sim 20$ meV) compared to the more stoichiometric films ($\sigma_{NBE} \sim 50$ meV), which corresponds to an open circuit voltage loss contribution that is nearly an order of magnitude lower. Such inhomogeneities can be attributed mainly to local variations of the Ga concentration. Hence, the differences between the samples could be explained by the different deposition times at elevated temperature allowing for different extents of homogeneity. Thus, Cu-poor films are not only favorable because of lower concentrations of deep defects but also because of reduced bandgap variations.

© 2023 Author(s). All article content, except where otherwise noted, is licensed under a Creative Commons Attribution (CC BY) license (http://creativecommons.org/licenses/by/4.0/). https://doi.org/10.1063/5.0145450

05 September 2023 12:41:40

I. INTRODUCTION

Si based solar cells are currently one of the main renewable energy sources, already providing 5% of the worldwide electricity in 2021.[1] The cost for PV modules has decreased dramatically over the last decades such that meanwhile the cost of the system components, as opposed to the absorber material, constitutes more than half of the total cost of a PV system.[2] These costs are largely proportional to the area of the system and thus increasing the efficiency of solar modules is the way forward to reduce cost. Currently, state-of-the-art Si solar cells have demonstrated a maximum efficiency of (26.7 ± 0.5)%,[3] which is approaching the theoretical maximum for single junction cells of ~31% given by the Shockley–Queisser limit.[4]

One way to considerably increase the efficiency of solar modules is through the use of tandem solar cells[5] where multiple semiconductor materials are stacked, with each efficiently converting photons from different portions of the solar spectrum. To couple with the widely used Si-based cells, materials that can absorb shorter wavelength, higher energy light efficiently, without thermalization losses, are required. The sulfide chalcopyrite $Cu(In,Ga)S_2$ (referred to as CIGS) is a direct bandgap semiconductor material, which is particularly interesting for such applications due to its direct bandgap and suitable bandgap energy, E_g, which can be tuned by alloying from 1.52 eV ($CuInS_2$) to 2.43 eV ($CuGaS_2$).[6] Additionally, chalcopyrites, in general, have demonstrated stable performance in real world conditions over decades. This makes it a promising candidate for the top cell in the tandem arrangement.

© Author(s) 2023

Furthermore, the relative ease of manufacturing and the limited toxicity of its constituent elements elevate the potential for CIGS.[7] Current state-of-the-art CIGS-based devices have demonstrated an efficiency of 15.5%,[8] lower than that of the related $Cu(In,Ga)Se_2$ (CIGSe) chalcopyrites.[9] In particular, the open circuit voltage deficit is higher in the sulfide chalcopyrites than in the selenide chalcopyrites. Thus, recent studies of CIGS have focused on minimizing non-radiative recombination[10,11] and on understanding electronic defects.[11,12] While there is limited information available in literature for recombination processes in $Cu(In,Ga)S_2$, comparison with the related CIGSe material system can offer valuable insights.

While a Ga gradient through the depth of the film is needed for efficient solar cell operation,[13,14] uncontrolled, compositional inhomogeneity has been found to be detrimental to cell performance. In particular, variations of the Ga/Ga + In ratio (GGI) lead to bandgap variations, lattice mismatch strain, and thus to tail states. These tail states increase radiative and non-radiative recombination, leading to a reduction in the open circuit voltage.[15–17] Deep in the gap these tail states take the form of Urbach tails with an exponential decay of the density of states, described by the Urbach energy. However, near the band edges the density of states is often dominated by a Gaussian distribution of bandgaps[18] with a width of σ_{E_g}. Analytical expressions exist, which link the *radiative* open circuit voltage loss, ΔV_{OC}^{rad}, to the Urbach energy[17] or the width of the distribution on bandgap.[19] Here, we estimate the width of the distribution of bandgaps from the width of the near band edge emission peak and so use the expression for Gaussian shaped density of states

$$\Delta V_{OC}^{rad} = \frac{{\sigma_{E_g}}^2}{2ek_BT}, \tag{1}$$

where e is the elementary charge and k_BT is the thermal energy.[19] It was shown for exponential tails that the open circuit voltage losses due to the non-radiative Shockley–Read–Hall recombination are of the same magnitude so that the total contribution, ΔV_{OC}, is approximately twice that obtained from Eq. (1).[17]

The origin of these detrimental bandgap fluctuations was found to be linked to variations in the GGI, as well as to variations in strain. Thermodynamic modeling of the ternary phase diagram revealed phase transitions, which are sensitive to small compositional variations under typical processing conditions, giving rise to lateral inhomogeneities.[20] Meanwhile, Avancini *et al.*[21] reported [Ga]/[Ga + In] (GGI) inhomogeneity in the vicinity of voids and crevices, possibly caused by variation in elemental diffusivities. Variation in surface GGI has also been detected due to rough surface topography with thicker regions allowing a greater distance over which the Ga concentration can increase (with a given Ga double gradient).[22] Szaniawski *et al.*[23] reported that changing the Cu-content of CIGSe films from a [Cu]/[Ga + In] (CGI) ratio of 1.0 to 0.5 led to reduction in the Ga gradient owing to the increase in the Cu vacancy (V_{Cu}) concentration and thus increased In and Ga diffusivities. This allowed for the (in this case desired) compositional differences through the thickness of the film to become more homogenized laterally. Furthermore, variations in strain, which can be caused by the different lattice constants of CIGS with different GGI,[24] also lead to variations in the bandgap.[25] The bandgap fluctuations could also be associated with the absorber deposition process. It is important to consider the different stages of growth kinetics and recrystallization in a complex multistage absorber deposition process.[21] Transition from Cu-rich to Cu-poor stage and annealing processes strongly influences the grain growth kinetics and microscopic elemental distribution, serving as a source of local GGI variation.

In this paper, lateral inhomogeneities within CIGS samples were investigated using cathodoluminescence scanning electron microscopy (CL-SEM). This technique allows for the direct comparison of the electro-optical properties of the CIGS samples to their morphology and grain structure on a nanometer scale.[26] Five samples of varying CGI ratios were studied using cathodoluminescence (CL), revealing different CL emission behaviors for different CGI ratios. The possible causes are discussed below.

II. METHODS

The details of the five $Cu(In,Ga)S_2$ samples are summarized in Table I. They were prepared using co-evaporation deposition. The CGI ratio of the films was varied from 0.93 to 1.29 while keeping the GGI ratio relatively constant (0.12–0.18). The number of deposition steps were also varied between samples. The bandgap energies were obtained using photoluminescence (PL) techniques.[10] We would like to point out that despite the usual error in x-ray spectroscopy (EDX) measurements the observed trends in CGI follow the expectations from the deposition experiments, i.e., higher CGI with shorter third stage, or no third stage as for sample E.[10] Furthermore, the trends observed in optoelectronic properties support the CGI trend.[10] Only sample D is different, in that it comes from a single stage process with constant fluxes. The difference in composition between samples C and D is not significant; both samples are nearly stoichiometric.

Cu-poor and Cu-rich $Cu(In,Ga)S_2$ thin films of ~2 μm thickness were deposited on sputtered Mo coated soda-lime glass (SLG) substrates by one-, two-, and three-stage co-evaporation process. For a one-stage process (sample D), Cu, In, Ga, and S were thermally co-evaporated at constant rate to form a film over the substrate with a growth temperature ~570 °C. In a two-stage process (sample E), In, Ga, and S were evaporated at substrate temperature of ~260 °C during the first stage followed by Cu–S evaporation at substrate temperature ~570 °C in the second stage. During the second stage, the transition to Cu-rich phase was monitored by the increase in the substrate heating power output along with the change in pyrometer reading due to the change in the emissivity of the absorber at the onset of Cu_xS formation beyond the stoichiometric composition. Note that here the Cu-rich film refers to the CIGS processed under excess Cu_xS phase and that the removal of Cu_xS renders the composition close to stoichiometry. For the three-stage process (sample A, B, and C), an additional third stage after Cu–S deposition was introduced, where In, Ga, and S were deposited at constant substrate temperature of ~570 °C. The process duration of the third stage was varied to obtain the desired CGI ratio of the final Cu-poor $Cu(In,Ga)S_2$ film. The sulfur partial pressure during the film growth was maintained in the range of 3×10^{-5}–7×10^{-5} mbar. Substrates were constantly rotated with the speed of 4 rpm throughout the growth process. After the growth, the substrates were cooled down

05 September 2023 12:41:40

© Author(s) 2023

TABLE I. A summary of the samples investigated in this study. The [Cu]/[Ga + In] ratio, the bandgap energy, $E_{g,PL}$, using PL at room temperature and the number of deposition steps used in the sample preparation are given.[10] Additionally, the performance of the best solar cells made from these absorbers[10] is presented. Note: these solar cells were made with different buffers and only the solar cell made from sample A was equipped with an anti-reflective coating; for details, see Ref. 10.

Sample	[Cu]/[Ga + In] ratio	$E_{g,PL}$ (eV)	Deposition	Eff (%)	V_{OC} (V)	j_{SC} (mA cm^2)	FF (%)
A	0.93	1.57	Three-stage	15.2	902	23.1	73
B	0.95	1.58	Three-stage	12.8	854	21.0	72
C	0.98	1.59	Three-stage	9.5	868	19.9	55
D	1.02	1.61	One-stage	No device – shunted			
E	1.29	1.58	Two-stage	6.7	607	18.5	60

in the presence of sulfur vapor until 140 °C to avoid the loss of sulfur from the film. The conducting Cu_xS phase formed at the surface of the Cu-rich absorbers were etched by dipping the sample in 10% aqueous KCN (potassium cyanide) solution for 5 min before characterization. A lower concentration KCN etching was performed on Cu-poor absorbers also (5% for 30 s).

The composition is acquired by energy dispersive x-ray spectroscopy (EDX) with beam energy of 20 kV on the as-grown absorbers before etching, that is, averaging over the ternary chalcopyrite phase and secondary copper sulfide (Cu_xS) phase. The chemical composition is this report is defined as the ratio [Cu]/[Ga] + [In], which involves the usual error of EDX of around 0.05 or more. Compositional profiles of sample B (typical for all Cu-poor samples) and E can be found in the supplementary material of Ref. 10.

The photoluminescence PL measurements were performed on a home-built set-up equipped with a 660 nm laser excitation source. Two off-axis parabolic mirrors are used to collect luminescence emitted from the samples, then focused into an optical fiber, and spectrally resolved by a monochromator. Eventually, the emission is detected by Si-CCD and (In,Ga)As photodiode array. The laser beam diameter and power are measured with a charge-coupled device camera and power meter, respectively, for use in the calibration of the photon flux. The calibration allows to set the incident photon flux from the excitation laser to the photon flux equal to above-bandgap photon flux for the material under an AM1.5 sun spectrum. Spectral corrections are performed utilizing the known spectrum of a calibrated halogen lamp. Quasi-Fermi level splitting (QFLS) is evaluated from the absolute intensity photoluminescence spectrum using a fit to generalized Planck's law.

The low temperature photoluminescence measurements were carried out in the above-mentioned system with the sample housed in a flow cryostat and cooled to liquid helium temperature.

Cathodoluminescence (CL) hyperspectral mapping was performed in an Attolight Allalin 4027 Chronos dedicated CL-SEM with a 150 l/mm and 500 nm blazed grating. All measurements were taken at room temperature with an electron beam acceleration voltage of 6.0 kV and a current of 3.0 nA with 90% of the beam energy being deposited within a depth of ~150 nm according to Monte Carlo CASINO simulations.[27] Initial CL images were observed to suffer from significant drift due to charging, so the samples were carbon-coated to improve the conduction of the beam electrons away from the surface. All data treatment was performed using the Python hyperspy library.[28]

III. RESULTS

The surface morphology, as measured by secondary electron (SE) imaging, of the five samples is shown in Fig. 1. For the three Cu-poor samples (CGI below 1), A, B, and C (all prepared using the three-stage deposition process), similar "classic" grain-like structures, akin to those found in other thin film solar cell materials, such as CdTe[29] and CIGSe,[30] are visible. For sample D, a rough surface topography with sharp angle surfaces and ridges can be seen. Finally, for sample E, small smooth, well-rounded structures separated by crevices are observed.

Figure 2 contains the mean CL spectra obtained from each of the five samples (averaged over the entire image areas shown in Fig. 1). Each sample shows a high emission peak between 1.55 and 1.70 eV, corresponding to the near-band-edge (NBE) transitions, and lower intensity peaks (labeled D1 and D2) at 1.30–1.40 eV, which we attribute to defect luminescence. It is seen that with increasing Cu-content, a general decrease in the NBE CL emission intensity (I_{NBE}) is observed. With the increase in the CGI ratio from 0.93 to 1.02, the I_{NBE} is reduced overall by approximately a factor of 6, with each step change between the samples roughly halving the NBE peak intensity. The CL spectra furthermore reveal a gradual increase in the mean NBE emission energy from sample A ($\langle E_{NBE} \rangle$ = 1.59 eV) to sample D ($\langle E_{NBE} \rangle$ = 1.66 eV). However, between samples D and E, there is no significant change in peak intensity and the emission energy decreases to $\langle E_{NBE} \rangle$ = 1.58 eV (a value similar to sample A). The trend in E_{NBE} between the different samples reflects the trend in E_g obtained using PL and is likely due to variations in the Ga content.[10] The small differences in the absolute values are attributed to differences in the utilized detectors (spectrally corrected vs uncorrected), large differences in sampling area (~150 nm for CL and multiple μm for PL) and excitation mechanism (especially sampling volume and excitation density). The excitation mechanism would be expected to play a particularly significant role due to the compositional grading perpendicular to the substrate, giving different mean compositions in the PL and CL sampled volumes. Finally, the full width at half maximum ($FWHM_{NBE}$) of the NBE

05 September 2023 12:41:40

© Author(s) 2023

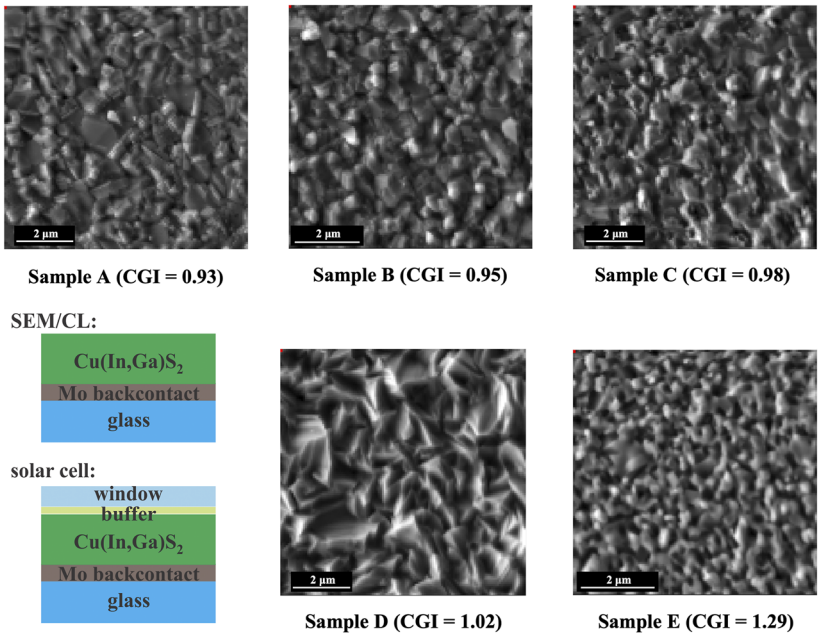

FIG. 1. Secondary Electron images of the top surfaces of the five samples studied (with increasing Cu-content from top left to bottom right). At the bottom left is a sketch of the sample structure. SEM and CL measurements were performed on the $Cu(In,Ga)S_2$ absorbers alone. All details about the solar cells can be found in Ref. 10.

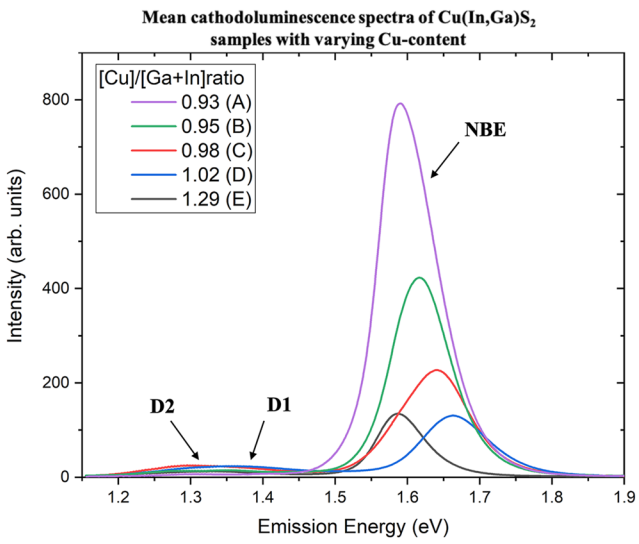

FIG. 2. The mean CL spectra of the five $Cu(In,Ga)S_2$ samples. The different measured optical transitions have been labeled NBE, D1, and D2, respectively.

TABLE II. A summary of the calculated mean NBE emission energy, $\langle E_{NBE} \rangle$, the full width half maximum ($FWHM_{NBE}$) of the NBE peak in the mean CL spectrum, the standard deviation of the NBE emission energies, σ_{NBE}, and the calculated radiative open circuit voltage loss, ΔV_{OC}, of the five CIGS samples.

Sample	CGI ratio	$\langle E_{NBE} \rangle$ (eV)	$FWHM_{NBE}$ (meV)	σ_{NBE} (meV)	ΔV_{OC} (mV)
A	0.93	1.596	95.4	21	20
B	0.95	1.616	95.0	19	20
C	0.98	1.627	115.7	52	110
D	1.02	1.663	112.1	45	80
E	1.29	1.588	80.4	18	10

peak was calculated for each sample and is summarized in Table II. The increase in the $FWHM_{NBE}$ values from samples A and B to C and D indicates the onset of a peak broadening mechanism while sample E shows diminished NBE peak width.

Figure 3 contains a panchromatic CL intensity image and a NBE emission energy image for each sample. Contrast in the panchromatic CL emission intensity can be expected as a result of various features within the sample. First, grain boundaries (GBs) act as sites for significant, undesirable non-radiative recombination, due to the increased presence of dislocations and bonding alterations,[31] and hence low CL intensity is expected to be seen here. Strictly, this only applies for random GBs as higher symmetry Σ3 twin GBs in CIGSe have been reported to give reduced rates of the detrimental non-radiative recombination[32] but the majority of the grain boundaries observed here in the CL contrast are likely to be random. The panchromatic CL intensity images in Fig. 3 (top row) show such variations in CL emission across the surface of each sample, with the bright regions as the grain interiors and the darker bands as

05 September 2023 12:41:40

© Author(s) 2023

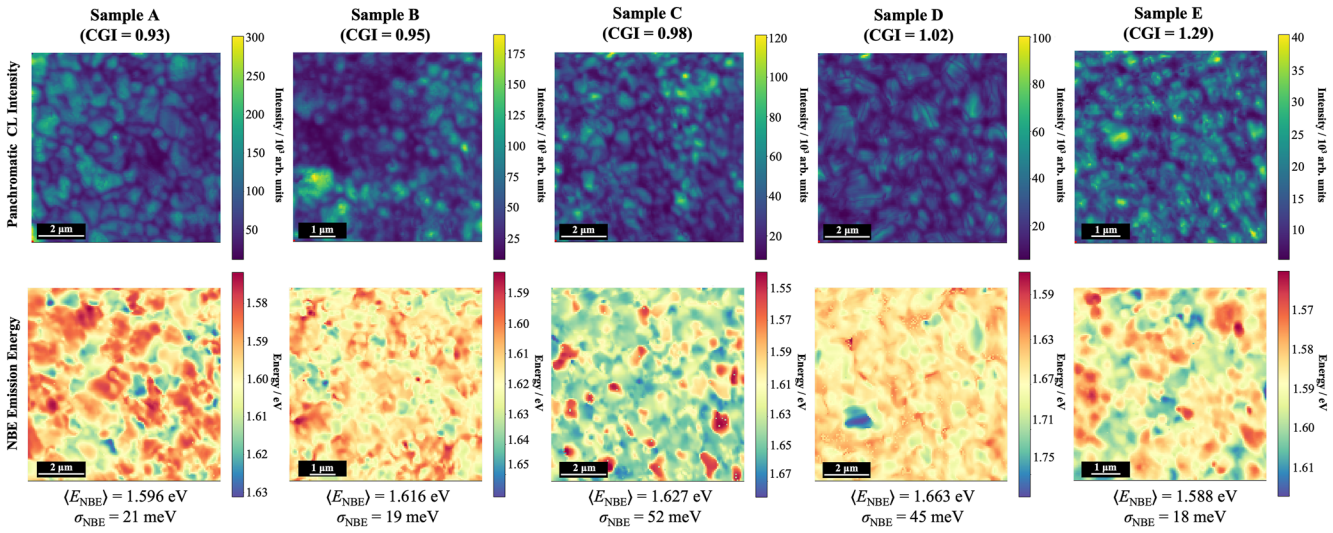

FIG. 3. Panchromatic (top) and NBE energy (bottom) images for the five $Cu(In,Ga)S_2$ samples (increasing CGI from left to right). Note the different scales for each image. The mean and standard deviation of E_{NBE} are also given for each sample. A color-blind friendly version of the figure can be found in supplementary material 3.

the GBs. Considering the different intensity scale bars, the same trend of decreasing CL intensity with increasing CGI between the samples, as in Fig. 2, can be seen. Comparison between these CL intensity images and the SE images in Fig. 1 shows that although some grain-like features seen in the SE image are reflected in the CL intensity images, the correlation between them is by no means perfect (see supplementary material 1). As the surface morphology seen in the SE images does not fully reveal the crystallography of the samples, henceforth the CL intensity images have been used to define the GBs. However, some of the differences between the locations of GBs suggested by the SEM and CL images might be due to the presence of Σ3 GBs that are mostly not detected in panchromatic images.[32]

Topographical features may also influence the CL intensities. Generally, regions with protruding surface features give reduced electron–hole pair generation (and hence decreased CL emission intensities) while regions with troughs and pits in turn give increased electron–hole pair generation. This is analogous to morphological effects on secondary electron emission coefficients as reported by Groudeva-Zotova *et al.*[33] The magnitude of this phenomenon is dependent on factors such as feature size and acceleration voltage. This can be seen in the panchromatic image for sample D where reduced intensity is seen along the ridges identified in Fig. 1 (see supplementary material 1), making the distinction between separate grains more difficult. However, such influences were not clearly identified in the panchromatic CL intensity images of the remaining samples. Additionally, this effect is not expected to significantly affect the CL emission energies and thus will not impact on the focus of this study.

To extract the center energies of the NBE emission peak, E_{NBE}, the CL spectrum was fitted using Gaussian functions at each pixel of the acquired hyperspectral dataset. The fitting results are summarized in the E_{NBE} images in Fig. 3 (bottom row). The equivalent overall trend of increasing mean NBE emission energy between the samples is reproduced, as in Fig. 2. For samples A, B, and E, small variations of the emission energy within each sample are observed. This can be characterized by calculating the standard deviations of the NBE energy (σ_{NBE}) and these were obtained as 21, 19, and 18 meV respectively, as summarized in Table II. However, for samples C and D, there are greater variations of emission energies within each sample with the σ_{NBE} calculated as 52 and 45 meV. Here, it is noted that σ_{NBE} is the calculated standard deviation of a random variable and not of a Gaussian distribution. The relative change in σ_{NBE} between the samples are greater than the calculated $FWHM_{NBE}$ values from the mean spectra (Fig. 2). This is due to the $FWHM_{NBE}$ of the mean spectrum being a measure of the mean disorder of the system convoluted by the intensity distribution between the disordered parts, while the standard deviation of the emission energy images is independent of the emission intensity distribution and is thus a more accurate representation of energy variations within the sample. However, the same overall trend of samples C and D exhibiting a greater variation (larger $FWHM_{NBE}$ and larger σ_{NBE}) in the NBE emission energy is still observed. Generally, there is no strong correlation seen between the E_{NBE} image with the topography (Fig. 1), as expected.[22] However, for sample D, where there was strong surface morphology influence on the panchromatic CL intensity images, the NBE emission energy is seen to increase along the previously identified ridges (see supplementary material 1). This effect is expected to be material driven though, not topography driven as was in the panchromatic CL intensity image.

We extracted line spectra across sample C (see Fig. 4) in order to better understand the nature of the NBE emission energy variation observed in our sample series. The position of the line spectra is marked in the panchromatic CL image in Fig. 4, with the line spectra themselves being shown in Figs. 4(a) and 4(b).

05 September 2023 12:41:40

© Author(s) 2023

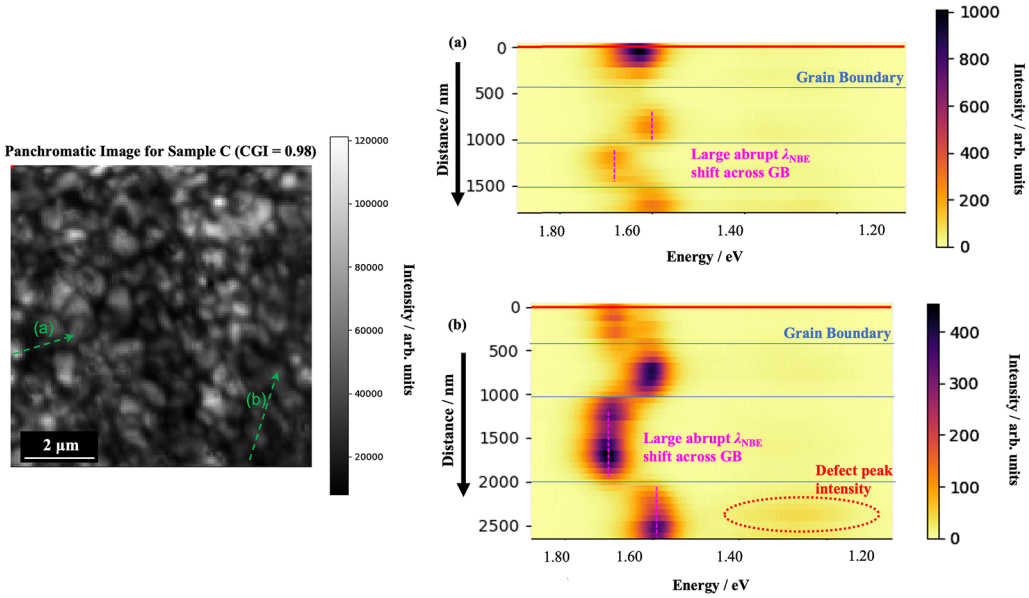

FIG. 4. A panchromatic CL intensity image (left) for sample C (CGI = 0.98) showing the positions and directions of line spectra (a) (top right) and (b) (bottom right). Note the different intensity scale used for each spectrum. Abrupt energy shifts and grain boundaries (as identified from the CL intensity image) are marked within the line spectra.

Both line spectra contain emission peaks at 1.65 and 1.55 eV and are drawn across multiple grain boundaries, which were identified in the panchromatic CL intensity images (Fig. 3) as lines of low emission intensity. The position of the grain boundaries is marked in both line spectra. It can be seen that the strongest emission energy shifts are abrupt at grain boundaries, shifting by as much as 100 meV. Some smaller, more gradual energy shifts can also be observed in some of the grains. Additionally, we can observe a variation in the defect luminescence intensity between the different grains.

IV. DISCUSSION

Observed NBE emission energy fluctuations are closely related to variations of the bandgap within the CIGS samples and can be quantitatively related to the open circuit voltage loss, as twice the radiative losses[19,50] given by Eq. (1) (shown in Table II). For the more homogeneous samples A, B, and E, this is limited to 10–20 mV, but for samples C and D, ΔV_{OC} is found to be around 100 mV. Due to the $\sigma_{E_g}{}^2$ relationship, the open circuit voltage loss increases by nearly an order of magnitude between samples, highlighting the importance of grasping the causes for this observed behavior. In fact, these calculated values for samples A and C are seen to account for most of the ~110 mV difference[10] in the losses in quasi-Fermi level splitting. The magnitude of the observed bandgap variation as well as the correlated ΔV_{OC} is well within the range reported by Mattheis *et al.*[51] (σ_{NBE} 10–90 meV and ΔV_{OC} up to 150 meV) in Cu(In,Ga)Se_2. Possible origins of such changes in the value of E_g across a material are compositional fluctuations, strain within the films or grain sizes.

For alloys such as Cu(In,Ga)S_2, the effect of the In and Ga compositions on the bandgap can be described quantitatively by interpolation[34]

$$E_g^{CuIn_{1-x}Ga_xS_2} = xE_g^{CuGaS_2} + (1-x)E_g^{CuInS_2} - bx(1-x), \quad (2)$$

where x is the GGI ratio, E_g^{CuInS2} = 1.52 eV, E_g^{CuGaS2} = 2.43 eV[6] and the bowing parameter, b = 0.2 eV.[34] Therefore, locally Ga-richer regions would have increased E_g and hence NBE transitions at higher energies, while In-richer regions would have decreased E_g and lower NBE transition energies.

Strains in deposited films may arise due to either a discrepancy in the materials' lattice constants or their thermal expansion coefficients. The prior case could arise if there were a sharp transition in GGI ratio between regions in the CIGS film, with In-richer domains having a larger equilibrium lattice constant and hence being in compression and the Ga-richer regions with reduced lattice constants being in tension. Films deposited at elevated temperatures can also experience mismatch strains due to the film and the substrate contracting by different amounts upon cooling. Generally, material under tensile strain would see a reduction in E_g, while material under compression would experience increased bandgaps.[35,36] However, for CIGS, this relationship is more complicated due to the splitting of the upper valence band with the heavy-hole like band becoming the highest valence band under compressive uniaxial stress and the light-hole like band under tensile stress.[25,37] For the samples studied here, the bandgap effects due to the lattice mismatch strains should not be significant as they also arise due to compositional inhomogeneities, but then its effects on the value of E_g, as described above, would be expected to dominate. In turn, it is unlikely for the lateral variations to be caused by the thermal expansion mismatch as

05 September 2023 12:41:40

© Author(s) 2023

for an isotropic film such strains would be expected to be uniform throughout.

Finally, if the grain sizes in a semiconductor material were smaller than the electron–hole wavefunction (i.e., 10 s of nanometers), quantum confinement effects could give an additional contribution and increase the bandgap of the material.[38] However, the features seen in the SE images in Fig. 1, as well as the regions of shifted E_{NBE} in Fig. 4, appear to be present across much larger length scales. The origins of lateral variations in cathodoluminescence emission energies are thus likely to be dominated by bandgap fluctuation due to GGI inhomogeneities,[39–41,51] though this will be expected to also give rise to lattice mismatch strains, which will give some contribution to E_g too.[21,36]

However, the source of such compositional inhomogeneity and the reason for the differences between samples of varying CGI are not currently clear. Bäcker *et al.*[42] found phase separation and dewetting in the precursor Cu–In–Ga film to be observed in the final CIGSe product. However, the multi-stage deposited CIGS films in this study were produced in a co-evaporation process.[10] As the overall GGI values were not varied significantly between samples, this would not be expected to give rise to the sample Cu precursor exhibiting increased phase separation as required for this theory. Therefore, any separation into In- and Ga-rich phases must take place upon the addition of Cu, but this is not thermodynamically predicted.[43]

Random alloy fluctuation as the driving force for spatial variation in the GGI ratio has been suggested by Mattheis *et al.*[51] who found that the bandgap variation observed for $Cu(In,Ga)Se_2$ layers strongly depends on the overall GGI ratio, having a maximum σ_{NBE} of about 90 meV at near equal Ga to In ratio. However, comparing the range of σ_{NBE} in our samples with the σ_{NBE} found by Mattheis *et al.*, we find that the GGI variation in our samples (0.12–0.18) is too small to explain the observed bandgap variation with random alloy fluctuations alone.

Elemental inhomogeneities in the vicinity of voids and crevices have also been observed,[21] but this is unlikely to be the cause of the large lateral E_{NBE} fluctuations seen, particularly for sample C where the variations can be seen grain-to-grain, as in Fig. 4. The GGI variations seen from the sample topography by Witte *et al.*[22] would expect to give rise to some correlation between the secondary electron and E_{NBE} images, even if precise film thickness variation cannot be determined from the prior. Furthermore, this relies upon the presence of the desirable Ga gradient perpendicular to the substrate, which was not detected by XRD for the single stage deposited sample D.[10] Therefore, it cannot explain the large E_{NBE} shifts seen for this sample.

In CIGSe films, it has been established that with deviations in composition away from stoichiometry, the atomic diffusivity increases due to the increased concentration of vacancy sites (V_{Cu} for Cu-poor films, V_{In} and V_{Ga} for Cu-rich films).[44] This allows for the greater In and Ga diffusivities in Cu-poorer films and thus the flatter (i.e., more homogeneous) Ga gradient perpendicular to the substrate, as reported by Szaniawski *et al.*[23] A similar trend is observed between the Cu-poor CIGS samples investigated here with increased lateral homogeneity for samples A and B that have compositions furthest from a CGI ratio = 1. This may suggest that the increased In and Ga diffusivities in these films allows for any uneven deposition of species to become more homogenized during growth whereas the more stoichiometric sample C is less successful in doing so, as characterized by the calculated σ_{NBE}. However, this would be expected to primarily affect the atomic mobility within grain interiors and cannot fully explain the increased homogeneity across grains that would require enhanced diffusion across grain boundaries too. Furthermore, this cannot be extended to sample E where the CIGS film achieves a narrow bandgap distribution while having a stoichiometric final film composition. Thus, this effect is not expected to be the main driving force for the differences in compositional homogeneity observed across these samples.

Finally, the kinetics of grain growth or recrystallization plays an important role in governing the film homogeneity. Three-stage deposition process typically proceeds through several stages of recrystallization, which depends on the deposition rate, duration, and temperature. It is well established that, in the case of CIGSe, an intermediate Cu-rich stage favors larger grain growth through Cu–Se assisted recrystallization,[45] stress relaxation,[46] and also alters the elemental diffusion profiles.[47–49] For fixed deposition rate and the temperature, as in the case of this study, duration becomes an important parameter governing the composition, gradient, and homogeneity. Since the final Cu-poor compositions were achieved by varying the duration of the third stage, comparison of samples A, B, and C allows us to directly correlate the effect of annealing times on film homogeneity. Caballero *et al.*[49] studied the effect of longer annealing times of the final (third) stage for CIGSe thin films. They showed smoother Ga/In gradient for longer annealed film as compared to standard films. A similar trend is observed here: an increased lateral homogeneity with increase in Cu-deficiency. A plausible explanation is that the longer annealing times assist in the grain growth and provide enough time to homogenize the distribution of the Ga and In species, resulting in smaller local bandgap variations. Additionally, prolonged annealing time could also lead to the growth of defect-poor grains at the expense of defect-rich grains as evidenced by higher intensity of the NBE emission for Cu-poor films. For the case of two-stage Cu-rich film (sample E), the improved lateral homogeneity can be attributed to the Cu–S assisted recrystallization process. Hence, Cu-poor films are not only beneficial in view of reduced defect density but also due to better lateral homogeneity.

V. CONCLUSION

In this study, scanning electron microscopy cathodoluminescence was used to study the opto-electric properties of five $Cu(In,Ga)S_2$ samples with varying CGI ratios. The near band edge peak intensity was found to increase ~6-fold by decreasing the CGI ratio for Cu-poor samples, with the overall trend in agreement with previous PL studies.[10] Their NBE emissions were also on average found to shift toward lower energies from $\langle E_{NBE} \rangle$ = 1.66 eV (CGI = 1.02) to $\langle E_{NBE} \rangle$ = 1.59 eV (CGI = 0.93). Analysis from fitting of the CL data revealed lateral, spatial variation in the emitted NBE energies across the surface of all five samples but were particularly prominent in the two near-stoichiometric samples C and D. The NBE emission energy standard deviation of 52 meV for sample C gives rise to a radiative loss in open circuit voltage, ΔV_{OC}, of 110 mV, which is nearly an order of magnitude greater than the one found for samples A, B, and E with less stoichiometric compositions.

05 September 2023 12:41:40

© Author(s) 2023

Meanwhile, sample A was found to have a total recombination open circuit voltage loss of 20 mV. Therefore, the open circuit voltage loss due to inhomogeneity can account for most of the ~110 mV difference seen in the loss of quasi-Fermi level splitting between samples A and C. Previously, the higher loss in films with higher Cu content was attributed to a deep defect seen in Cu-rich films.[10] This seems still to be the case for the most Cu-rich sample (E), which has a narrow distribution of band gaps, but still a large loss in quasi-Fermi level splitting. The new investigations presented here, on the other hand, support that lateral GGI fluctuations are the main cause of differences in the loss in quasi-Fermi level splitting and thus the open circuit voltage loss in Cu-poor films. It should be noted, though, that even the best films had a rather large loss in quasi-Fermi level splitting so that the role of deep defects still needs to be investigated. The observed lateral fluctuations were attributed to GGI inhomogeneities that were alleviated for the Cu-poor samples A and B due to the increased deposition times at elevated temperatures required to reach their desired CGI ratios. Hence, due to the higher CL emission intensities and greater lateral homogeneity, Cu-poor CIGS films offer most promise for high efficiency solar cell applications.

SUPPLEMENTARY MATERIAL

In the supplementary material, we show animated overlays of Figs. 1 and 3 for samples A and D to demonstrate the correlation between morphology, NBE emission energy, and emission intensity. Furthermore, we show the histogram of NBE energy for all five samples.

ACKNOWLEDGMENTS

We thank the Luxembourgish Fond National de la Recherche (FNR) for funding in the framework of the MASSENA (Project No. PRIDE 15/10935404), as well as the REACH (Project No. INTER/UKRI/20/15050982). Rachel Oliver and Gunnar Kusch also acknowledge funding from the EPSRC under Grant No. EP/V029231/1.

AUTHOR DECLARATIONS

Conflict of Interest

The authors have no conflicts to disclose.

Author Contributions

Sean Peedle: Formal analysis (lead); Investigation (lead); Writing – original draft (lead). **Damilola Adeleye**: Investigation (equal); Methodology (equal); Writing – review & editing (supporting). **Sudhanshu Shukla**: Conceptualization (equal); Investigation (equal); Writing – original draft (supporting); Writing – review & editing (equal). **Susanne Siebentritt**: Conceptualization (equal); Formal analysis (equal); Funding acquisition (equal); Project administration (equal); Resources (equal); Supervision (equal); Writing – original draft (equal); Writing – review & editing (equal). **Rachel Oliver**: Conceptualization (equal); Funding acquisition (equal); Project administration (equal); Resources (equal); Supervision (equal); Writing – original draft (supporting); Writing – review & editing (supporting). **Gunnar Kusch**: Conceptualization (equal); Formal analysis (equal); Investigation (equal); Methodology (equal); Software (equal); Writing – original draft (equal); Writing – review & editing (equal).

DATA AVAILABILITY

The data that support the findings of this study are openly available in the University of Cambridge repository under https://doi.org/10.17863/CAM.100224.

REFERENCES

[1] IEA-PVPS, Trends in Photovoltaic Applications 2022, IEA-PVPS, 2022, https://iea-pvps.org/trends_reports/trends-2022/.

[2] S. Philipps and W. Warmuth, Photovoltaics Report, 2023, https://www.ise.fraunhofer.de/en/publications/studies/photovoltaics-report.html.

[3] M. A. Green, E. D. Dunlop, J. Hohl-Ebinger, M. Yoshita, N. Kopidakis, and A. W. Y. Ho-Baillie, "Solar cell efficiency tables (Version 55)," Prog. Photovoltaics **28**, 3–15 (2020).

[4] S. Beeby and N. White, *Energy Harvesting for Autonomous Systems* (Artech House, 2010).

[5] S. Albrecht and B. Rech, "Perovskite solar cells: On top of commercial photovoltaics," Nat. Energy **2**, 16196 (2017).

[6] R. Scheer and H. W. Schock, *Chalcogenide Photovoltaics: Physics, Technologies, and Thin Film Devices* (John Wiley & Sons, 2011).

[7] R. Kaigawa, A. Neisser, R. Klenk, and M. C. Lux-Steiner, "Improved performance of thin film solar cells based on $Cu(In,Ga)S_2$," Thin Solid Films **415**, 266–271 (2002).

[8] H. Hiroi, Y. Iwata, S. Adachi, H. Sugimoto, and A. Yamada, "New world-record efficiency for pure-sulfide $Cu(In,Ga)S_2$ thin-film solar cell with Cd-free buffer layer via KCN-free process," IEEE J. Photovoltaics **6**(3), 760 (2016).

[9] M. Nakamura, K. Yamaguchi, Y. Kimoto, Y. Yasaki, T. Kato, and H. Sugimoto, "Cd-free $Cu(In,Ga)(Se,S)_2$ thin-film solar cell with record efficiency of 23.35%," IEEE J. Photovoltaics **9**(6), 1863–1867 (2019).

[10] S. Shukla, M. Sood, D. Adeleye, S. Peedle, G. Kusch, D. Dahliah, M. Melchiorre, G. Rignanese, G. Hautier, R. Oliver, and S. Siebentritt, "Over 15% efficient wide-band-gap $Cu(In,Ga)S_2$ solar cell: Suppressing bulk and interface recombination through composition engineering," Joule **5**, 1816 (2021).

[11] A. Lomuscio, T. Rödel, T. Schwarz, B. Gault, M. Melchiorre, D. Raabe, and S. Siebentritt, "Quasi-Fermi-level splitting of Cu-poor and Cu-rich $CuInS_2$ absorber layers," Phys. Rev. Appl. **11**, 054052 (2019).

[12] A. Lomuscio, M. Sood, M. Melchiorre, and S. Siebentritt, "Phonon coupling and shallow defects in $CuInS_2$," Phys. Rev. B **101**, 085119 (2020).

[13] A. M. Gabor, J. R. Tuttle, D. S. Albin, M. A. Contreras, R. Noufi, and A. M. Hermann, "High-efficiency $CuIn_xGa_{1-x}Se_2$ solar cells from $(In_x,Ga_{1-x})Se_3$ precursor films," Appl. Phys. Lett. **65**, 198 (1994).

[14] T. Feurer, B. Bissig, T. P. Weiss, R. Carron, E. Avancini, J. Löckinger, S. Buecheler, and A. N. Tiwari, "Single-graded CIGS with narrow bandgap for tandem solar cells," Sci. Technol. Adv. Mater. **19**(1), 263–270 (2018).

[15] J. H. Werner, J. Mattheis, and U. Rau, "Efficiency limitations of polycrystalline thin film solar cells: Case of $Cu(In,Ga)Se_2$," Thin Solid Films **480-481**, 399–409 (2005).

[16] U. Rau, B. Blank, T. C. M. Müller, and T. Kirchartz, "Efficiency potential of photovoltaic materials and devices unveiled by detailed-balance analysis," Phys. Rev. Appl. **7**, 044016 (2017).

[17] M. H. Wolter, R. Carron, E. Avancini, B. Bissig, T. P. Weiss, S. Nishiwaki, T. Feurer, S. Buecheler, P. Jackson, W. Witte, and S. Siebentritt, "How

05 September 2023 12:41:40

© Author(s) 2023

band tail recombination influences the open-circuit voltage of solar cells," Prog. Photovoltaics **30**, 702 (2021).
[18]G. Rey, G. Larramona, S. Bourdais, C. Choné, B. Delatouche, A. Jacob, G. Dennler, and S. Siebentritt, "On the origin of band-tails in kesterite," Sol. Energy Mater. Sol. Cells **179**, 142–151 (2018).
[19]U. Rau and J. H. Werner, "Radiative efficiency limits of solar cells with lateral band-gap fluctuations," Appl. Phys. Lett. **84**, 3735 (2004).
[20]C. P. Muzzillo, C. E. Campbell, and T. J. Anderson, "Cu–Ga–In thermodynamics: Experimental study, modeling, and implications for photovoltaics," J. Mater. Sci. **51**, 3362–3379 (2016).
[21]E. Avancini, D. Keller, R. Carron, Y. Arroyo-Rojas Dasilva, R. Erni, A. Priebe, S. Di Napoli, M. Carrisi, G. Sozzi, R. Menozzi, F. Fu, S. Buecheler, and A. N. Tiwari, "Voids and compositional inhomogeneities in Cu(In,Ga)Se_2 thin films: Evolution during growth and impact on solar cell performance," Sci. Technol. Adv. Mater. **19**, 871 (2018).
[22]W. Witte, D. Abou-Ras, K. Albe, G. H. Bauer, F. Bertram, C. Boit, R. Brüggemann, J. Christen, J. Dietrich, A. Eicke, D. Hariskos, M. Maiberg, R. Mainz, M. Meessen, M. Müller, O. Neumann, T. Orgis, S. Paetel, J. Pohl, H. Rodriguez-Alvarez, R. Scheer, H. W. Schock, T. Unold, A. Weber, and M. Powalla, "Gallium gradients in Cu(In,Ga)Se_2 thin film solar cells," Prog. Photovoltaics **23**, 717–733 (2015).
[23]P. Szaniawski, P. Salomé, V. Fjällström, T. Törndahl, U. Zimmermann, and M. Edoff, "Influence of varying Cu content on growth and performance of Ga-graded Cu(In,Ga)Se_2 solar cells," IEEE J. Photovoltaics **5**(6), 1775 (2015).
[24]S. Schäfer, H. Stange, J. A. Márquez, C. Genzel, and R. Mainz, "Stress formation during In–Ga interdiffusion in thin-film $CuIn_{1-x}Ga_xSe_2$ absorber layers leads to stable Ga gradients," Phys. Rev. Appl. **14**, 024063 (2020).
[25]S. Shirakata, S. Isomura, and S. Chichibu, "Photoreflectance characterization of lattice strain in wide-gap Cu-III-VI_2 epitaxial layers," Trans. Mater. Res. Soc. Jpn. **20**, 782 (1996).
[26]B. G. Yacobi and D. B. Holt, "Cathodoluminescence scanning electron microscopy of semiconductors," J. Appl. Phys. **59**(4), R1 (1986).
[27]D. Drouin, A. R. Couture, D. Joly, X. Tastet, V. Aimez, and R. Gauvin, "CASINO V2.42—A fast and easy-to-use modeling tool for scanning electron microscopy and microanalysis users," Scanning **29**, 92–101 (2007).
[28]F. de la Peña, E. Prestat, V. T. Fauske, P. Burdet, T. Furnival, P. Jokubauskas, M. Nord, T. Ostasevicius, K. E. MacArthur, D. N. Johnstone, M. Sarahan, J. Lähnemann, J. Taillon, Pquinn-dls, T. Aarholt, V. Migunov, A. Eljarrat, J. Caron, S. Mazzucco, B. Martineau, S. Somnath, T. Poon, M. Walls, T. Slater, actions-user; N. Tappy, N. Cautaerts, F. Winkler, G. Donval, and J. C. Myers, Zenodo (2020), hyperspy/hyperspy: Release v1.6.1..
[29]C. Doroody, K. S. Rahman, S. F. Abdullah, M. N. Harif, H. N. Rosly, S. K. Tiong, and N. Amin, "Temperature difference in close-spaced sublimation (CSS) growth of CdTe thing film on ultra-thin glass substrate," Results Phys. **18**, 103213 (2020).
[30]N. Barreau, J. Lähnemann, F. Couzinié-Devy, L. Assmann, P. Bertoncini, and J. Kessler, "Impact of Cu-rich growth on the $CuIn_{1-x}Ga_xSe_2$ surface morphology and related solar cells behaviour," Sol. Energy Mater. Sol. Cells **93**, 2013–2019 (2009).
[31]L. L. Kazmerski, "Micro- to nano-characterization of semiconductor grain boundaries," Surf. Sci. Rep. **19**, 169–189 (1993).
[32]M. Müller, D. Abou-Ras, T. Rissom, F. Bertram, and J. Christen, "Symmetry dependent optoelectronic properties of grain boundaries in polycrystalline Cu(In,Ga)Se_2 thin films," J. Appl. Phys. **115**, 023514 (2014).
[33]S. Groudeva-Zotova, W. Jacob, and A. von Keudell, "Secondary electron emission coefficient of C:H and Si:C thin films and some relations to their morphology and composition," Diamond Relat. Mater. **5**, 1087–1095 (1996).
[34]I. V. Bodnar and A. I. Lukomskii, "The concentration dependence of the band gap for $CuGa_xIn_{1-x}S_2$ and $AgGa_xIn_{1-x}S_2$ solid solutions," Phys. Status Solidi A **98**(2), K165–K169 (1986).
[35]C. P. Kuo, S. K. Vong, R. M. Cohen, and G. B. Stringfellow, "Effect of mismatch strain on band gap in III-V semiconductors," J. Appl. Phys. **57**, 5428 (1985).
[36]J. K. Larsen, L. Gütay, Y. Aida, and S. Siebentritt, "Spatial variations of optoelectronic properties in single crystalline $CuGaSe_2$ thin films studied by photoluminescence," Thin Solid Films **519**, 7332–7336 (2011).
[37]S. Theodoropoulou, D. Papadimitriou, A. G. Mamalis, D. E. Manolakos, R. Klenk, and M. Lux-Steiner, "Band-gap energies and strain effects in $CuIn_{1-x}Ga_xS_2$ based solar cells," Semicond. Sci. Technol. **22**, 933–940 (2007).
[38]O. D. Neikov and N. A. Yefimov, *Handbook of Non-Ferrous Metal Powders: Technologies and Applications*, 2nd ed. (Elsevier, 2019).
[39]M. Krause, A. Nikolaeva, M. Maiberg, P. Jackson, D. Hariskos, W. Witte, J. A. Márquez, S. Levcenko, T. Unold, R. Scheer, and D. Abou-Ras, "Microscopic origins of performance losses in highly efficient Cu(In,Ga)Se_2 thin-film solar cells," Nat. Commun. **11**, 4189 (2020).
[40]R. G. Wilks, I. Repins, M. A. Contreras, R. Félix, J. Herrero-Albillos, L. Tati-Bismaths, F. Kronast, R. Noufi, and M. Bär, "Intergrain variations of the chemical and electronic surface structure of polycrystalline Cu(In,Ga)Se_2 thin-film solar cell absorbers," Appl. Phys. Lett. **101**, 103908 (2012).
[41]L. Gütay and G. H. Bauer, "Spectrally resolved photoluminescence studies on Cu(In,Ga)Se_2 solar cells with lateral submicron resolution," Thin Solid Films **515**, 6212–6216 (2007).
[42]J. P. Bäcker, S. S. Schmidt, H. Rodriguez-Alvarez, C. Wolf, C. A. Kaufmann, M. Hartig, R. Mainz, and R. Schlatmann, "Lateral phase separation in Cu–In–Ga precursor and Cu(In,Ga)Se_2 absorber thin films," Sol. Energy Mater. Sol. Cells **162**, 120–126 (2017).
[43]A. Thomere, C. Guillot-Deudon, M. T. Caldes, R. Bodeux, N. Barreau, S. Jobic, and A. Lafond, "Chemical crystallographic investigation on Cu_2S–In_2S_3–Ga_2S_3 ternary system," Thin Solid Films **665**, 46–50 (2018).
[44]O. Lundberg, J. Lu, A. Rockett, M. Edoff, and L. Stolt, "Diffusion of indium and gallium in Cu(In,Ga)Se_2 thin film solar cells," J. Phys. Chem. Solids **64**, 1499–1504 (2003).
[45]R. Mainz, E. Simsek Sanli, H. Stange, D. Azulay, S. Brunken, D. Greiner, S. Hajaj, M. D. Heinemann, C. A. Kaufmann, M. Klaus, Q. M. Ramasse, H. Rodriguez-Alvarez, A. Weber, I. Balberg, O. Millo, P. A. van Aken, and D. Abou-Ras, "Annihilation of structural defects in chalcogenide absorber films for high-efficiency solar cells," Energy Environ. Sci. **9**, 1818–1827 (2016).
[46]R. Mainz, H. Rodriguez-Alvarez, M. Klaus, D. Thomas, J. Lauche, A. Weber, M. D. Heinemann, S. Brunken, D. Greiner, C. A. Kaufmann, T. Unold, H. W. Schock, and C. Genzel, "Sudden stress relaxation in compound semiconductor thin films triggered by secondary phase segregation," Phys. Rev. B **92**, 155310 (2015).
[47]T. Nishimura, S. Toki, H. Sugiura, K. Nakada, and A. Yamada, "Interfacial quality improvement of Cu(In,Ga)Se_2 thin film solar cells by Cu-depletion layer formation," Appl. Phys. Express **9**, 092301 (2016).
[48]Y. Kamikawa, J. Nishinaga, S. Ishizuka, T. Tayagaki, H. Guthrey, H. Shibata, K. Matsubara, and S. Niki, "Effect of thermal annealing on the redistribution of alkali metals in Cu(In,Ga)Se_2 solar cells on glass substrate," J. Appl. Phys. **123**, 093101 (2018).
[49]R. Caballero, C. A. Kaufmann, V. Efimova, T. Rissom, V. Hoffmann, and H. W. Schock, "Investigation of Cu(In,Ga)Se_2 thin-film formation during the multi-stage co-evaporation process," Prog. Photovoltaics **21**(1), 30–46 (2013).
[50]J. Mattheis, U. Rau, and J. H. Werner, "Light absorption and emission in semiconductors with band gap fluctuations—A study on Cu(In,Ga)Se_2 thin films," J. Appl. Phys. **101**, 113519 (2007).
[51]J. Mattheis, T. Schlenker, M. Bogicevic, U. Rau, and J. H. Werner, "Band gap fluctuations in Cu(In,Ga)Se_2 thin films," MRS Online Proc. Libr. **865**, 164 (2004).

05 September 2023 12:41:40

© Author(s) 2023